Biomechanical Modelling of Sitting Movements for Designing Robotic Lower-Limb Prostheses and Exoskeletons with Energy Regeneration

Brock Laschowski[1]
Department of Systems Design Engineering,
University of Waterloo,
Waterloo, Canada
Email: blaschow@uwaterloo.ca

Reza Sharif Razavian
Department of Bioengineering,
Imperial College London,
London, England
Email: r.sharif-razavian@imperial.ac.uk

John McPhee
Department of Systems Design Engineering,
University of Waterloo,
Waterloo, Canada
Email: mcphee@uwaterloo.ca

[1] Brock Laschowski, Department of Systems Design Engineering, University of Waterloo, Ontario, N2L 3G1, Canada. Email: blaschow@uwaterloo.ca. Telephone: (519) 888-4567.

ABSTRACT

BACKGROUND: Regenerative powertrain systems can extend the operating durations of robotic lower-limb prostheses and exoskeletons. These energy-efficient biomechatronic devices have been exclusively designed and evaluated for level-ground walking. Building on previous investigations, this research assessed the lower-limb joint biomechanical powers during stand-to-sit movements using inverse dynamics modelling to estimate the biomechanical energy available for electrical regeneration. METHODS: Nine participants performed 20 sitting and standing movements while lower-limb kinematics and ground reaction forces were measured. Following the biomechanical model design, dynamic parameter identification computed the subject-specific body segment inertial parameters that minimized the differences in ground reaction forces and moments between the experimental measurements and inverse dynamic simulations. Joint biomechanical powers were calculated from net joint torques and rotational velocities and numerically integrated over time to determine biomechanical energy. RESULTS: The hip joint generated the largest maximum negative biomechanical power (1.8 ± 0.5 W/kg), followed by the knee joint (0.8 ± 0.3 W/kg) and ankle joint (0.2 ± 0.1 W/kg). Negative biomechanical energy from the hip, knee, and ankle joints per stand-to-sit movement were 0.36 ± 0.06 J/kg, 0.16 ± 0.08 J/kg, and 0.03 ± 0.01 J/kg, respectively. CONCLUSIONS: Using previously published maximum energy regeneration efficiencies (i.e., approximately 37 %), robotic knee prostheses and exoskeletons could theoretically regenerate 0.06 ± 0.03 J/kg of electrical energy while sitting down. These findings have implications on design optimization of regenerative powertrains for energy-efficient lower-limb biomechatronic devices.

Keywords: biomechanics, biomechatronics, exoskeletons, prosthetics, regenerative braking, rehabilitation, robotics

1. BACKGROUND

Over 12 million individuals in the United States alone have mobility impairments resulting from stroke, spinal cord injury, and other neuromusculoskeletal conditions [1]. There are approximately 2 million Americans with limb amputations [2]. These numbers are expected to significantly increase with the emergent aging population and growing incidences of cancer and diabetes [1-3]. Robotic lower-limb prostheses and exoskeletons can enable geriatric and rehabilitation patients to perform common movements (e.g., sit-to-stand) that necessitate net positive mechanical power by mimicking their amputated or unimpaired biological muscle actuators [4-9]. However, these biomechatronic devices have typically required significant amounts of electrical power and large onboard batteries to facilitate daily functioning (e.g., rechargeable lithium-polymer or lithium-ion batteries) [5-6, 10-11]. For instance, the maximum electrical power consumption of robotic knee prostheses during level-ground walking has averaged 43 ± 30 W [4]. Robotic knee prostheses under research and development have provided 3.1 ± 2.2 hours of average operation and weighed 4.0 ± 1.1 kg [4, 6]. The Össur Power Knee, the only commercially-available powered knee prosthesis, weighs approximately 3.2 kg and provides 5-7 hours of continuous functioning. Robotic lower-limb exoskeletons have provided 1-5 hours of maximum operation [1]. Portable electrical power has been considered one of the leading challenges to developing robotic lower-limb exoskeletons for real-world environments [1, 10-11].

Consequently, barring advances in onboard energy storage devices like ultracapacitors, investigations into energy-efficient biomechatronic design and control systems are warranted.

Regenerative braking, also called energy regeneration, represents a promising solution to the aforementioned shortcomings. Human joints can generate negative biomechanical power (i.e., braking) and positive biomechanical power (i.e., motoring) [12]. The net joint torques and rotational velocities have opposing polarities during braking, and the same polarities during motoring. During "natural cadence" level-ground walking, the human knee joint primarily resembles a damper mechanism, performing net negative mechanical work via energy dissipation, and the ankle joint mainly resembles an actuating motor, performing net positive mechanical work and generating forward propulsion, particularly during stance-phase push-off [5, 10-12]. These characteristic human walking biomechanics are illustrated in Figure 1. Note that joint biomechanical power calculations inherently assume joint torque generators that are independent of adjacent joints, therein overlooking the behavior of biarticular muscles spanning multiple joints (e.g., simultaneously provide energy generation at one joint and energy dissipation at another) [12].

Analogous to electric and hybrid electric vehicles [13-14], several biomechatronic knee designs have incorporated regenerative powertrains to convert the otherwise dissipated joint biomechanical energy during legged locomotion into electrical energy for recharging the onboard batteries while

providing negative mechanical work for controlled system deceleration [5, 15-29]. These energy-efficient powertrains can enable lighter onboard batteries and/or extend the operating durations between recharging. Consequently, regenerating energy could 1) benefit rehabilitation patients in developing countries without accessible electricity for battery recharging [30-31], and 2) support the development of more sophisticated control technologies (e.g., machine vision and deep learning [32]) that have traditionally required significant computing power. Relating to socket-suspended lower-limb prostheses, minimizing onboard battery weight via energy regeneration could reduce musculoskeletal pain occurrences associated with excessive tugging on the human-prosthesis interface [2].

Previous investigations of lower-limb prostheses and exoskeletons with regenerative powertrains have focused exclusively on level-ground walking [15-29, 33-35]. However, geriatric and rehabilitation patients often exhibit slower walking speeds (e.g., 24 % speed reduction from 25 to 75 years age) and take fewer steps/day (e.g., 75 % reduction from 60 to 85 years age) [3], therein limiting the potential for energy regeneration during level-ground walking. In contrast, sitting and standing movements are seemingly more representative activities of clinical populations and therefore should be considered when designing such biomechatronic devices. The average human performs approximately 60 sitting and standing movements each day [36]. Several robotic lower-limb prostheses and exoskeletons have been designed and evaluated for

sitting and standing movements (example shown in Figure 2) [7-9, 36-42]. Regenerating energy while performing stand-to-sit movements represents an unexplored and potentially effective auxiliary method to level-ground walking for recharging the onboard batteries of robotic lower-limb prostheses and exoskeletons. Preceding the mechatronic design and optimization of regenerative powertrains (i.e., backdriveable actuator-transmission systems), studying the human movement biomechanics is needed. Accordingly, this research investigated the lower-limb joint biomechanical powers during stand-to-sit movements using inverse dynamics modelling to estimate the joint biomechanical energy available for electrical regeneration.

2. METHODS

2.1 Motion Capture Experiments

Building on previous investigations, which often involved fewer than 3 participants [7, 38-39, 41-42], this research included 9 participants (height: 180 ± 4 cm, weight: 78 ± 7 kg, age: 25 ± 3 years, sex: male). Informed written consent was obtained, and the University of Waterloo Office of Research Ethics approved this research. Each participant performed 20 sitting and standing movements, using self-selected rates, while lower-limb kinematics and ground reaction forces were measured with optical motion capture cameras and synchronized force plates, respectively (see Figure 3). The seat height resembled that from previous research (i.e., approximately 46 cm) [43-44]. Prior to experimental data collection, the imaging system was calibrated, and the global

coordinate system specified. The motion capture cameras (Optotrak, Northern Digital Incorporation, Canada) provided 3D measurements of active marker positions in global coordinates. Active marker systems are generally considered the gold standard in human movement biomechanics [45]. The optical motion capture cameras and force plates were sampled at 100 Hz and 300 Hz, respectively. For tracking individual body segment positions in the sagittal plane, virtual markers were digitized overlying palpable anatomical landmarks on the right lower-limb, including the lateral malleolus, lateral femoral and tibial condyles, and greater trochanter. These virtual marker positions correspond with those recommended by the International Society of Biomechanics [45].

2.2 Data Processing

Missing marker data were estimated using cubic spline interpolations. The ankle and hip joint centers were assumed to coincide with the lateral malleolus and greater trochanter virtual markers, respectively. The estimated knee joint center was the midpoint between the lateral femoral and tibial condyle virtual markers [45]. Piecewise cubic hermite interpolating polynomials were used for resampling and time-normalizing the kinematic measurements. The line vectors between the ankle and knee joint centers, and knee and hip joint centers, defined the shank and thigh body segment lengths, respectively (see Figure 4). Inverse kinematics determined the generalized coordinates through vector algebra, therein converting the virtual marker positions to independent joint coordinates. The ankle joint angle was the angle between the shank body

segment and horizontal axis. The relative angle between the shank and thigh body segments defined the knee joint angle. Further consideration was needed for calculating the hip joint angle. Given the relative rotations between the pelvis and HAT body segment (i.e., pelvis tilting), the measured marker-cluster rotations differed from HAT segment rotations during stand-to-sit movements. To resolve these discrepancies, the HAT segment was assumed vertical when standing upright (i.e., initial posture) and seated (i.e., final posture) and the pelvis angle rotations were assumed to progress linearly with time throughout stand-to-sit movements. The relative angle between the thigh and HAT body segments defined the hip joint angle. Joint angles were filtered using 10th-order low-pass Butterworth filters with 5 Hz cut-off frequencies and zero-phase digital filtering [12]. Joint rotational velocities and accelerations were computed by numerically differentiating the joint angles.

Similar to previous research [37], smoothed pelvis translational velocities, which were approximated from the marker-cluster shown in Figure 3, were used for defining the sitting and standing movement durations. These kinematic measurements were filtered using 10th-order low-pass Butterworth filters and 3 Hz cut-off frequencies, followed by zero-phase digital filtering and moving average smoothing filtering. Sitting and standing movement durations were defined when the smoothed pelvis translational velocities exceeded some subject-specific percentage of their maximum values; optimal percentages were approximated through trial-and-error simulations for consistent results. Other

investigations have used changes in vertical ground reaction forces [36, 44] and knee and hip joint kinematics [40-41] for defining the sitting and standing movement durations. The force plate measurements were filtered using 10th-order low-pass Butterworth filters with 30 Hz cut-off frequencies and zero-phase digital filtering [12]. The force plate measurements were subject to piecewise cubic hermite interpolating polynomials for time-normalization.

2.3 Biomechanical Model Design

The human biomechanical system was dynamically modelled using MapleSim software (Maplesoft, Canada). The biomechanical model comprised a two-dimensional (sagittal-plane) inverted triple-pendulum with shank, thigh, and HAT rigid body segments (see Figure 4). The foot segment was fixed to the inertial ground frame [43-44]. The ankle, knee, and hip joints were modelled as revolute kinematic pairs. Biological passive elastic joint torques, including stiffness and damping, were ignored since we assumed idealized joints for lower-limb prosthetic applications. Frictionless joints ensured that only net joint torques performed mechanical work. The biomechanical model had three degrees-of-freedom and was represented using three generalized coordinates (i.e., ankle, knee, and hip joint angles) with zero algebraic constraints. Since the foot segment was fixed to the inertial frame, the ground reaction forces and moments coincided with the ankle joint reaction forces and torques. Body segment centers of mass were reported relative to distal joint centers and moments of inertia about the center of mass positions. The ground reaction

forces measured underneath the seat were applied to the biomechanical model buttocks when seated. The multibody system equations for inverse dynamics modelling comprised only algebraic equations. MapleSim automatically generated these system equations symbolically using graph-theoretic algorithms, therein enabling computationally-efficient dynamic simulations. Figure 5 shows the linear graph representation of the biomechanical model. Joint biomechanical powers were calculated from net joint torques and rotational velocities (i.e., $P_J = \tau_J \cdot \omega_J$) and numerically integrated over time to determine joint biomechanical energy during stand-to-sit movements.

2.4 Dynamic Parameter Identification

Accurate system parameters are needed for effective dynamic modelling and simulation in robotics engineering and human movement biomechanics. Human body segment parameters have been approximated using various methods, including medical imaging [46-48], dynamic parameter identification [49], and anthropometric proportionalities from cadaver dissections [50]. Dynamic parameter identification can be subcategorized into offline methods (e.g., experimental measurements and system input-output matching) and online methods (e.g., neural networks and nonlinear adaptive control algorithms) [51]. This research used offline dynamic parameter identification. The biomechanical model was driven using the experimental joint kinematics and seat forces. The ankle, knee, and hip joint torques, and ground reaction forces and moments underneath the foot, were calculated from inverse dynamic simulations. The

dynamic parameter identification used constrained nonlinear programming (Fmincon, MATLAB) and an interior-point algorithm to approximate the unknown subject-specific body segment inertial parameters (i.e., mass, center of mass, and moment of inertia). Similar to previous research [43], the optimization computed the parameters wherein the squared differences in ground reaction forces (GRF) and moments (GRM) between the experimental measurements and inverse dynamic simulations at each time step (i) were minimized. The optimization multiobjective function was

$$J = \sum_{\mathrm{i}} \mathrm{w}_1 (\mathrm{GRF}_{\mathrm{measure}}[\mathrm{i}] - \mathrm{GRF}_{\mathrm{model}}[\mathrm{i}])^2 \times \frac{1}{(\mathrm{BW})^2} + \sum_{\mathrm{i}} \mathrm{w}_2 \left((\mathrm{GRM}_{\mathrm{measure}}[\mathrm{i}] + \mathrm{GRM}_{\mathrm{offset}}) - \mathrm{GRM}_{\mathrm{model}}[\mathrm{i}] \right)^2 \times \frac{1}{(\mathrm{H} \times \mathrm{BW})^2}$$

where GRF included both horizontal (x) and vertical (y) components, GRM was about z-axis, BW was the participant bodyweight, coefficient H = 1 meter, and $\mathrm{GRM}_{\mathrm{offset}}$ compensated for the horizonal distance between the foot location and force plate center ($\mathrm{GRM}_{\mathrm{offset}} = \mathrm{GRF}_{\mathrm{y}} \cdot \mathrm{footlocation}$). The optimization variables were shank, thigh, and HAT body segment mass, center of mass, and moment of inertia. Other variables included "$\mathrm{seat}_{\mathrm{offset}}$" and "footlocation". $\mathrm{Seat}_{\mathrm{offset}}$ was the horizontal distance between the biomechanical model buttocks (i.e., vertical seat force point-of-application) and estimated hip joint center. The optimization was constrained by setting 1) lower and upper bounds on individual variables, and 2) the summed body segment masses equal the experimentally measured total bodyweight. Initial guesses were taken from human anthropometrics and/or

were midpoints between the upper and lower bounds. Each term in the multiobjective optimization had equal weights (i.e., $w_1=w_2$). Stopping criteria for the optimization step size and objective function changes were both 1e-8 between iterations. Similar parameter identification methods have been used in robotics engineering [51]. The experimental and computational methods are summarized in Figure 6.

3. RESULTS

Table 1 presents the maximum and minimum hip, knee, and ankle joint angles, torques, and biomechanical powers. The movement durations were time-normalized to enable between and within participant averaging [12]. Dynamic variables (i.e., net joint torques and biomechanical powers) were also normalized to participant bodyweight. Subjective feedback from the participants indicated that performing stand-to-sit movements were significantly more challenging than sit-to-stand movements, particularly from a balance control perspective. The biomechanical measurements were uploaded to IEEE DataPort [link] and are publicly available for download. To the authors' knowledge, there exists no previously published database on stand-to-sit biomechanics. Figure 7 presents the calculated hip, knee, and ankle joint angles during sitting movements from inverse kinematics. Decreasing joint angles indicate hip flexion, knee extension, and ankle dorsiflexion. Increasing joint angles indicate hip extension, knee flexion, and ankle plantar flexion. The uncertainties represent ± one standard deviation across all participants (n=9) and trials (20 trials/participant). There

were minimal between and within participant inconsistencies in joint kinematics, as demonstrated by the small standard deviations.

The calculated hip, knee, and ankle joint torques from inverse dynamic simulations are presented in Figure 8. The maximum net joint torques about the hip, knee, and ankle were 0.7 ± 0.1 Nm/kg, 1.1 ± 0.3 Nm/kg, and 0.4 ± 0.1 Nm/kg, respectively. Figure 9 presents the calculated hip, knee, and ankle joint biomechanical powers during stand-to-sit movements. The hip joint generated the largest maximum net negative biomechanical power (1.8 ± 0.5 W/kg), followed by the knee joint (0.8 ± 0.3 W/kg) and ankle joint (0.2 ± 0.1 W/kg). Net positive mechanical work, also called concentric work, was performed when the biomechanical power trajectories were positive. When the biomechanical power trajectories were negative, eccentric or negative mechanical work was performed by the net joint torques [12]. Numerically integrating negative joint biomechanical power over time, the calculated negative biomechanical energy from the hip, knee, and ankle joints per stand-to-sit movement were 0.36 ± 0.6 J/kg, 0.16 ± 0.8 J/kg, and 0.03 ± 0.01 J/kg, respectively.

4. DISCUSSION

Analogous to electric and hybrid electric vehicles [13-14], regenerative braking can extend the operating durations of robotic lower-limb prostheses and exoskeletons by converting the otherwise dissipated joint biomechanical energy during negative work movements into electrical energy via backdriving the onboard actuator-transmission system. Whereas previous investigations have

focused exclusively on level-ground walking [15-29, 33-35], this research computed the lower-limb joint biomechanical energy available for electrical regeneration during stand-to-sit movements. The sitting and standing movement biomechanics of nine participants were experimentally measured. A customized lower-limb biomechanical model was designed, and dynamic parameter identification was used to approximate subject-specific body segment inertial parameters for inverse dynamics. The calculated maximum net negative biomechanical powers from the hip, knee, and ankle joints were 1.8 ± 0.5 W/kg, 0.8 ± 0.3 W/kg, and 0.2 ± 0.1 W/kg, respectively. In comparison, previous experimental measurements of robotic lower-limb prostheses during sitting and standing movements reported approximately 0.7-0.8 W/kg maximum knee joint mechanical power [36, 41]. The strong quantitative agreement between the current (0.8 ± 0.3 W/kg) and previous (0.7-0.8 W/kg) [36, 41] maximum knee joint mechanical powers, normalized to participant bodyweight, supported the model validation.

Negative joint biomechanical power was numerically integrated over time to determine the biomechanical energy available for electrical regeneration while sitting down. The average net negative mechanical work from the hip, knee, and ankle joints were 0.36 ± 0.06 J/kg, 0.16 ± 0.8 J/kg, and 0.03 ± 0.01 J/kg, respectively, during one stand-to-sit movement. Although the hip performed the most net negative mechanical work, the knee joint should instead be considered for regenerative powertrain system designs given the increased structural

complexity of the biological hip (i.e., more degrees-of-freedom). Coincidentally, most lower-limb biomechatronic devices with energy regeneration have involved knee-centered designs [5, 15-29, 33-35]. Using previously published maximum energy regeneration efficiencies (i.e., approximately 37 %) [16], robotic knee prostheses and exoskeletons could theoretically regenerate 0.06 ± 0.03 J/kg of electrical energy per stand-to-sit movement. In comparison, previous electromechanical knee prostheses have regenerated approximately 0.13 J/kg of maximum electrical energy per stride during "comfortable" level-ground walking speeds, respectively [16]. Consequently, regenerating energy during stand-to-sit movements presents a potential auxiliary method to level-ground walking for recharging the onboard batteries of robotic lower-limb prostheses and exoskeletons.

Quantifying the biomechanical power and joint torque requirements during sitting and standing movements can provide improved design specifications for lower-limb biomechatronic devices. Sit-to-stand movements are physically demanding and require joint torque generation for accelerating the human biomechanical system upwards. Stand-to-sit movements require braking joint torques for controlled system deceleration. Using subject-specific inverse dynamics modelling, this research computed maximum hip, knee, and ankle joint torques during stand-to-sit movements of approximately 0.7 ± 0.1 Nm/kg, 1.1 ± 0.3 Nm/kg, and 0.4 ± 0.1 Nm/kg, respectively. In comparison, previous investigations involving the mechatronic design and evaluation of lower-limb

exoskeletons and prostheses for sitting and standing movements reported maximum knee joint torques ranging from 0.8-1.0 Nm/kg [36, 38-40]. The relatively good quantitative agreement between the current (1.1 ± 0.3 Nm/kg) and previous (0.8-1.0 Nm/kg) [36, 38-40] maximum normalized knee joint torques for sitting and standing movements further supported the model validation. Whereas many previous investigations have focused on sit-to-stand movements [8-9, 38-40, 42-44], the biomechanics of stand-to-sit movements has received limitation attention. Therefore, alongside informing the mechatronic design and optimization of regenerative powertrains for lower-limb prostheses and exoskeletons, the current research also contributes towards increasing the general knowledge of human movement biomechanics.

This research included "able-bodied" participants without any known movement impairments. Conversely, rehabilitation patients using passive assistive devices typically perform sitting and standing movements with significant inter-limb biomechanical asymmetries, wherein the unimpaired lower-limb is disproportionally used for mechanical power and joint torque generation [6-7, 36-38]. Such disproportionate mechanical loading over time could bring about osteoarthritis and other osteodegenerative diseases. Robotic lower-limb prostheses and exoskeletons can facilitate more effective (i.e., symmetric) sitting and standing movement biomechanics via mimicking their amputated or unimpaired biological muscle actuators. For example, previous research studying unilateral transfemoral amputees performing sit-to-stand movements reported

that maximum vertical ground reaction forces were 58 ± 14 % asymmetric using passive knee prostheses and 19 ± 12 % asymmetric using robotic counterparts [36]. For stand-to-sit movements, maximum vertical ground reaction forces were 48 ± 16 % and 28 ± 12 % asymmetric using the passive and robotic knee prostheses, respectively [36]. In addition to excluding such inter-limb biomechanical asymmetries, this research also excluded upper-limb support structures, which are common among geriatric patients (e.g., walkers and canes) and affect the movement biomechanics. Future investigations should therefore include geriatric and/or rehabilitation patients to account for potential differences in sitting and standing movement biomechanics compared to able-bodied individuals.

The highest reported maximum energy regeneration efficiency with lower-limb biomechatronic devices for rehabilitation patients was achieved by Andrysek and colleagues [16] without using computational methods like dynamic modelling and optimization during the design process. However, there are numerous degrees-of-freedom in the mechatronic design space that can facilitate regenerative braking with robotic lower-limb prostheses and exoskeletons. For instance, assuming a given powertrain topology (example shown in Figure 10), the mechanical power transmission, electromagnetic actuator, and energy storage device each comprise system parameters that could be optimized to maximize electrical regeneration for an applied biomechanical load [5, 25]. Since most powertrain system parameters and components are mechanically and/or

electromechanically interconnected, determining optimal energy-efficient system designs through experimental trial-and-error can be time-consuming and ineffective [5, 25]. Consequently, extending the current research, a regenerative powertrain model will be developed and integrated into the human lower-limb biomechanical model. The resulting biomechatronic system model will enable 1) sensitivity analyses of powertrain system design parameters (e.g., transmission ratios) and components (e.g., batteries vs. ultracapacitors) to evaluate their respective contributions to regeneration, and 2) powertrain design parameter optimization for maximizing energy regeneration without affecting the human movement biomechanics and energetics [15, 24-25, 28, 35].

5. CONCLUSION

Regenerative powertrain systems can convert the otherwise dissipated joint biomechanical energy during negative work movements into electrical energy for recharging lower-limb biomechatronic devices (i.e., prostheses and exoskeletons). Whereas previous investigations have focused exclusively on level-ground walking, this research involved the dynamic modelling and measurement of human sitting movements to estimate the joint biomechanical energy available for electrical regeneration. The calculated net joint torques and biomechanical powers from inverse dynamic simulations agreed with previous experimental measurements with robotic lower-limb prostheses and exoskeletons, therein supporting the model validation. The computed net negative biomechanical energy from the hip, knee, and ankle joints were 0.36 ±

0.06 J/kg, 0.16 ± 0.8 J/kg, and 0.03 ± 0.01 J/kg, respectively, during one stand-to-sit movement. Using previously published maximum energy regeneration efficiencies (i.e., approximately 37 %), robotic knee prostheses and exoskeletons could theoretically regenerate 0.06 ± 0.03 J/kg of electrical energy while sitting down. Moving forward, a regenerative powertrain model will be developed and integrated into the human lower-limb biomechanical model. The resulting biomechatronic system model will provide a novel computational framework for design optimization of regenerative powertrain systems.

ABBREVIATIONS

P: Joint mechanical power; τ: Joint torque; θ: Joint angle; ω and $\dot{\theta}$: Joint rotational velocity; $\ddot{\theta}$: Joint rotational acceleration; GRM: Ground reaction moment; GRF: Ground reaction force; BW: Bodyweight; H: Height; F_{seat}: Seat contact forces; p: Body segment inertial parameters; VI: Electrical power.

ETHICS DECLARATION

Informed written consent was obtained, and the University of Waterloo Office of Research Ethics approved this research.

CONSENT FOR PUBLICATION

Not applicable.

AVAILABILITY OF DATA AND MATERIALS

The biomechanical measurements generated and/or analyzed were uploaded to IEEE DataPort [link] and are publicly available for download. To the authors' knowledge, there exists no previously published database on stand-to-sit movement biomechanics.

COMPETING INTERESTS

The authors declare that they have no competing interests.

FUNDING

This research was funded by the Natural Sciences and Engineering Research Council of Canada (NSERC) and Dr. John McPhee's Canada Research Chair in Biomechatronic System Dynamics. These funding agencies did not influence the

study design, collection, analysis, and interpretation of data, and/or manuscript writing.

AUTHOR CONTRIBUTIONS

BL managed the study design, literature review, participant recruitment, motion capture experiments, biomechanical model design, kinematics data processing, inverse kinematics, inverse dynamics, dynamic parameter identification, data analyses and interpretation, and manuscript writing. RS contributed towards the kinematics data processing, dynamic parameter identification, and manuscript writing. JM contributed towards the data interpretation and manuscript writing. All authors read and approved the final manuscript.

ACKNOWLEDGMENTS

The authors thank Dr. Stacey Acker (Department of Kinesiology, University of Waterloo, Canada) and Mark Charlet (Department of Engineering Physics, Université Laval, Canada) for supporting the experimental measurements.

REFERENCES

[1] Young AJ, Ferris DP. State of the art and future directions for lower limb robotic exoskeletons. IEEE Transactions on Neural Systems and Rehabilitation Engineering. 2017;25(2):171-182.

[2] Maryniak A, Laschowski B, Andrysek J. Technical overview of osseointegrated transfemoral prostheses: Orthopedic surgery and implant design centered. ASME Journal of Engineering and Science in Medical Diagnostics and Therapy. 2018;1(2):020801-020801-7.

[3] Grimmer M, Riener R, Walsh CJ, Seyfarth A. Mobility related physical and functional losses due to aging and disease - A motivation for lower limb exoskeletons. Journal of NeuroEngineering and Rehabilitation. 2019;16.

[4] Laschowski B, Andrysek J. Electromechanical design of robotic transfemoral prostheses. In: ASME International Design Engineering Technical Conferences and Computers and Information in Engineering Conference. Quebec City, Canada; 2018. p. V05AT07A054.

[5] Laschowski B, McPhee J, Andrysek J. Lower-limb prostheses and exoskeletons with energy regeneration: Mechatronic design and optimization review. ASME Journal of Mechanisms and Robotics. 2019;11(4):040801-040801-8.

[6] Pieringer DS, Grimmer M, Russold MF, Riener R. Review of the actuators of active knee prostheses and their target design outputs for activities of daily living. In: IEEE International Conference on Rehabilitation Robotics. London, UK; 2017. p. 1246-1253.

[7] Simon AM, Fey NP, Ingraham KA, Young AJ, Hargrove LJ. Powered prosthesis control during walking, sitting, standing, and non-weight bearing activities using neural and mechanical inputs. In: Proceedings of International IEEE/EMBS Conference on Neural Engineering. San Diego, USA; 2013. p. 1174-1177.

[8] Skelton J, Wu SK, Shen X. Design of a powered lower-extremity orthosis for sit-to-stand and ambulation assistance. ASME Journal of Medical Devices. 2013;7(3):030910-030910-2.

[9] Thapa S, Zheng H, Kogler GF, Shen X. A robotic knee orthosis for sit-to-stand assistance. In: ASME Dynamic Systems and Control Conference. Minneapolis, USA; 2016. p. V001T07A004.

[10] Dollar AM, Herr H. Active orthoses for the lower-limbs: Challenges and state of the art. In: IEEE International Conference on Rehabilitation Robotics. Noordwijk, Netherlands; 2007. p. 968-977.

[11] Dollar AM, Herr H. Lower extremity exoskeletons and active orthoses: Challenges and state-of-the-art. IEEE Transactions on Robotics. 2008;24(1):144-158.

[12] Winter DA. The Biomechanics and Motor Control of Human Gait: Normal, Elderly, and Pathological. Waterloo Biomechanics, Canada; 1998.

[13] Razavian R, Azad NL, McPhee J. On real-time optimal control of a series hybrid electric vehicle with an ultra-capacitor. In: American Control Conference. Montreal, Canada; 2012. p. 547-552.

[14] Rizzoni G, Peng H. Hybrid and electrified vehicles: The role of dynamics and control. ASME Mechanical Engineering Magazine. 2013;135(03):S10-S17.

[15] Andrysek J, Chau G. An electromechanical swing-phase-controlled prosthetic knee joint for conversion of physiological energy to electrical energy: Feasibility study. IEEE Transactions on Biomedical Engineering. 2007;54(12):2276-2283.

[16] Andrysek J, Liang T, Steinnagel B. Evaluation of a prosthetic swing-phase controller with electrical power generation. IEEE Transactions on Neural Systems and Rehabilitation Engineering. 2009;17(4):390-396.

[17] Barto T, Simon D. Neural network control of an optimized regenerative motor drive for a lower-limb prosthesis. In: American Control Conference. Seattle, USA; 2017. p. 5330-5335.

[18] Bolivar E, Rezazadeh S, Gregg R. A general framework for minimizing energy consumption of series elastic actuators with regeneration. In: ASME Dynamic Systems and Control Conference. Tysons, USA; 2017. p. V001T36A005.

[19] Donelan JM, Li Q, Naing V, Hoffer JA, Weber DJ, Kuo AD. Biomechanical energy harvesting: Generating electricity during walking with minimal user effort. Science. 2008;319(5864):807-810.

[20] Donelan JM, Naing V, Li Q. Biomechanical energy harvesting. In: IEEE Radio and Wireless Symposium. San Diego, USA; 2009. p. 1-4.

[21] Gualter Dos Santos E, Richter H. Modeling and control of a novel variable-stiffness regenerative actuator. In: ASME Dynamic Systems and Control Conference. Atlanta, USA; 2018. p. V002T24A003.

[22] Khalaf P, Warner H, Hardin E, Richter H, Simon D. Development and experimental validation of an energy regenerative prosthetic knee controller and prototype. In: ASME Dynamic Systems and Control Conference. Atlanta, USA; 2018. p. V001T07A008.

[23] Kim BH, Richter H. Energy regeneration-based hybrid control for transfemoral prosthetic legs using four-bar mechanism. In: Annual Conference of the IEEE Industrial Electronics Society. Washington, USA; 2018. p. 2516-2521.

[24] Li Q, Naing V, Hoffer JA, Weber DJ, Kuo AD, Donelan JM. Biomechanical energy harvesting: Apparatus and method. In: IEEE International Conference on Robotics and Automation. Pasadena, USA; 2008. p. 3672-3677.

[25] Li Q, Naing V, Donelan JM. Development of a biomechanical energy harvester. Journal of NeuroEngineering and Rehabilitation. 2009;6(22).

[26] Rarick R, Richter H, Van Den Bogert A, Simon D, Warner H, Barto T. Optimal design of a transfemoral prosthesis with energy storage and regeneration. In: American Control Conference. Portland, USA; 2014. p. 4108-4113.

[27] Rohani F, Richter H, Van Den Bogert AJ. Optimal design and control of an electromechanical transfemoral prosthesis with energy regeneration. PLoS ONE. 2017;12(11):e0188266.

[28] Tucker MR, Fite KB. Mechanical damping with electrical regeneration for a powered transfemoral prosthesis. In: IEEE/ASME International Conference on Advanced Intelligent Mechatronics. Montreal, Canada; 2010. p. 13-18.

[29] Warner H, Simon D, Richter H. Design optimization and control of a crank-slider actuator for a lower-limb prosthesis with energy regeneration. In: IEEE International Conference on Advanced Intelligent Mechatronics. Banff, Canada; 2016. p. 1430-1435.

[30] Arelekatti VNM, Winter AG. Design of a fully passive prosthetic knee mechanism for transfemoral amputees in India. In: IEEE International Conference on Rehabilitation Robotics. Singapore, Singapore; 2015.

[31] Arelekatti VNM, Winter AGV. Design and preliminary field validation of a fully passive prosthetic knee mechanism for users with transfemoral amputation in India. ASME Journal of Mechanisms and Robotics. 2018;10(3):031007-031007-8.

[32] Laschowski B, McNally W, Wong A, McPhee J. Preliminary design of an environment recognition system for controlling robotic lower-limb prostheses and exoskeletons. In: IEEE International Conference on Rehabilitation Robotics. Toronto, Canada; 2019. p. 868-873.

[33] Khademi G, Richter H, Simon D. Multi-objective optimization of tracking/impedance control for a prosthetic leg with energy regeneration. In: IEEE Conference on Decision and Control. Las Vegas, USA; 2016. p. 5322-5327.

[34] Khademi G, Mohammadi H, Richter H, Simon D. Optimal mixed tracking/impedance control with application to transfemoral prostheses with energy regeneration. IEEE Transactions on Biomedical Engineering. 2018;65(4):894-910.

[35] Riemer R, Shapiro A. Biomechanical energy harvesting from human motion: Theory, state of the art, design guidelines, and future directions. Journal of NeuroEngineering and Rehabilitation. 2011;8:22.

[36] Simon AM, Fey NP, Ingraham KA, Finucane SB, Halsne EG, Hargrove LJ. Improved weight-bearing symmetry for transfemoral amputees during standing up and sitting down with a powered knee-ankle prosthesis. Archives of Physical Medicine and Rehabilitation. 2016;97(7):1100-1106.

[37] Gao F, Zhang F, Huang H. Investigation of sit-to-stand and stand-to-sit in an above knee amputee. In: Annual International Conference of the IEEE Engineering in Medicine and Biology Society. Boston, USA; 2011. p. 7340-7343.

[38] Shepherd MK, Rouse EJ. Design and characterization of a torque-controllable actuator for knee assistance during sit-to-stand. In: Annual International Conference of the IEEE Engineering in Medicine and Biology Society. Orlando, USA; 2016. p. 2228-2231.

[39] Shepherd MK, Rouse EJ. Design and validation of a torque-controllable knee exoskeleton for sit-to-stand assistance. IEEE/ASME Transactions on Mechatronics. 2017;22(4):1695-1704.

[40] Vantilt J, Tanghe K, Afschrift M, Bruijnes A, Junius K, Geeroms J, Aertbeliën E, De Groote F, Lefeber D, Jonkers I, De Schutter J. Model-based control for exoskeletons with series elastic actuators evaluated on sit-to-stand movements. Journal of NeuroEngineering and Rehabilitation. 2019;16:65.

[41] Varol HA, Sup F, Goldfarb M. Powered sit-to-stand and assistive stand-to-sit framework for a powered transfemoral prosthesis. In: IEEE International Conference on Rehabilitation Robotics. Kyoto, Japan; 2009. p. 645-651.

[42] Wu M, Haque MR, Shen X. Sit-to-stand control of powered knee prostheses. In: ASME Design of Medical Devices Conference. Minneapolis, USA; 2017. p. V001T05A015.

[43] Norman-Gerum V, McPhee J. Comparison of cylindrical wrapping geometries to via points for modeling muscle paths in the estimation of sit-to-stand muscle forces. In: ASME International Design Engineering Technical Conferences and Computers and Information in Engineering Conference. Portland, USA; 2013. p. V07AT10A011.

[44] Norman-Gerum V, McPhee J. Constrained dynamic optimization of sit-to-stand motion driven by Bézier curves. ASME Journal of Biomechanical Engineering. 2018;140(12):121011.

[45] Razavian RS, Greenberg S, McPhee J. Biomechanics imaging and analysis. Encyclopedia of Biomedical Engineering. 2019. p. 488-500.

[46] Durkin JL, Dowling JJ, Scholtes L. Using mass distribution information to model the human thigh for body segment parameter estimation. ASME Journal of Biomechanical Engineering. 2005;127(3):455-464.

[47] Laschowski B, McPhee J. Body segment parameters of Paralympic athletes from dual-energy X-ray absorptiometry. Sports Engineering. 2016;19(3):155-162.

[48] Laschowski B, McPhee J. Quantifying body segment parameters using dual-energy X-ray absorptiometry: A Paralympic wheelchair curler case report. Procedia Engineering. 2016;147:163-167.

[49] Kulic D, Venture G, Yamane K, Demircan E, Mizuuchi I, Mombaur K. Anthropomorphic movement analysis and synthesis: A survey of methods and applications. IEEE Transactions on Robotics. 2016;32(4):776-795.

[50] De Leva P. Adjustments to Zatsiorsky-Seluyanov's segment inertia parameters. Journal of Biomechanics. 1996;29(9):1223-1230.

[51] Wu J, Wang J, You Z. An overview of dynamic parameter identification of robots. Robotics and Computer-Integrated Manufacturing. 2010;26(5):414-419.

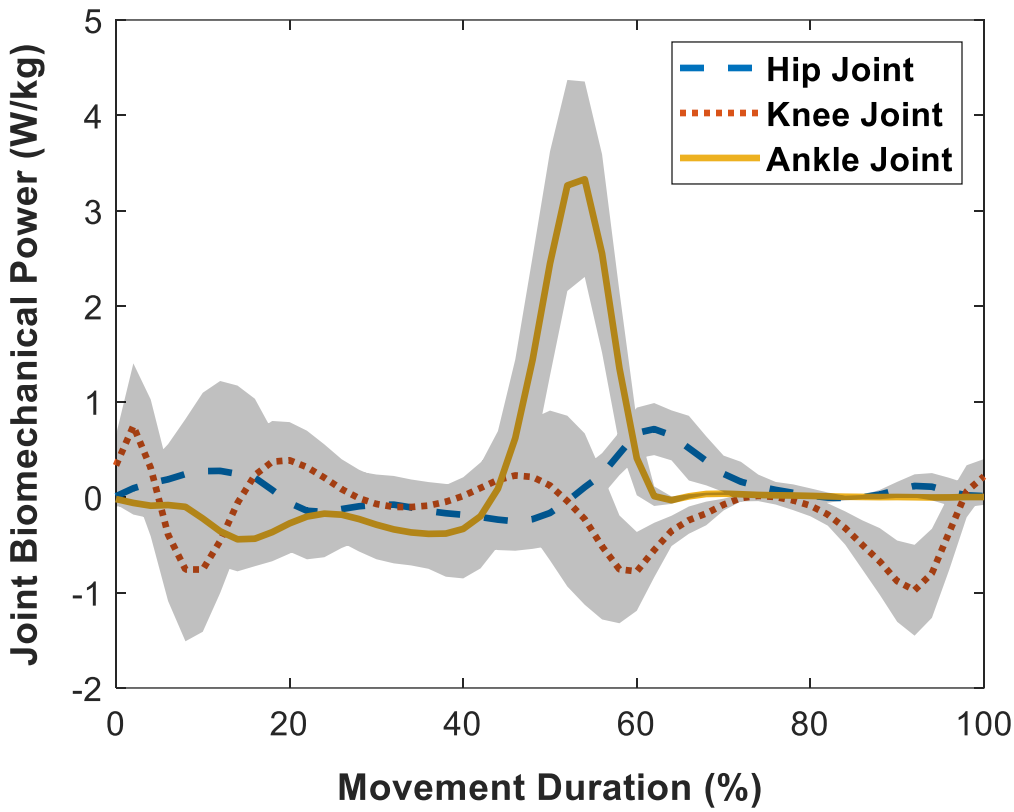

Figure 1. Estimated hip, knee, and ankle joint biomechanical powers during one "natural cadence" level-ground walking stride, normalized to participant bodyweight. Data were taken from Winter [12]. The uncertainties represent ± one standard deviation across different participants (n=19). The movement trajectories commenced at heel-strike.

Figure 2. Example of a robotic lower-limb exoskeleton for assisting human sitting and standing movements. Photograph attained from Dr. Elliott Rouse (University of Michigan, USA).

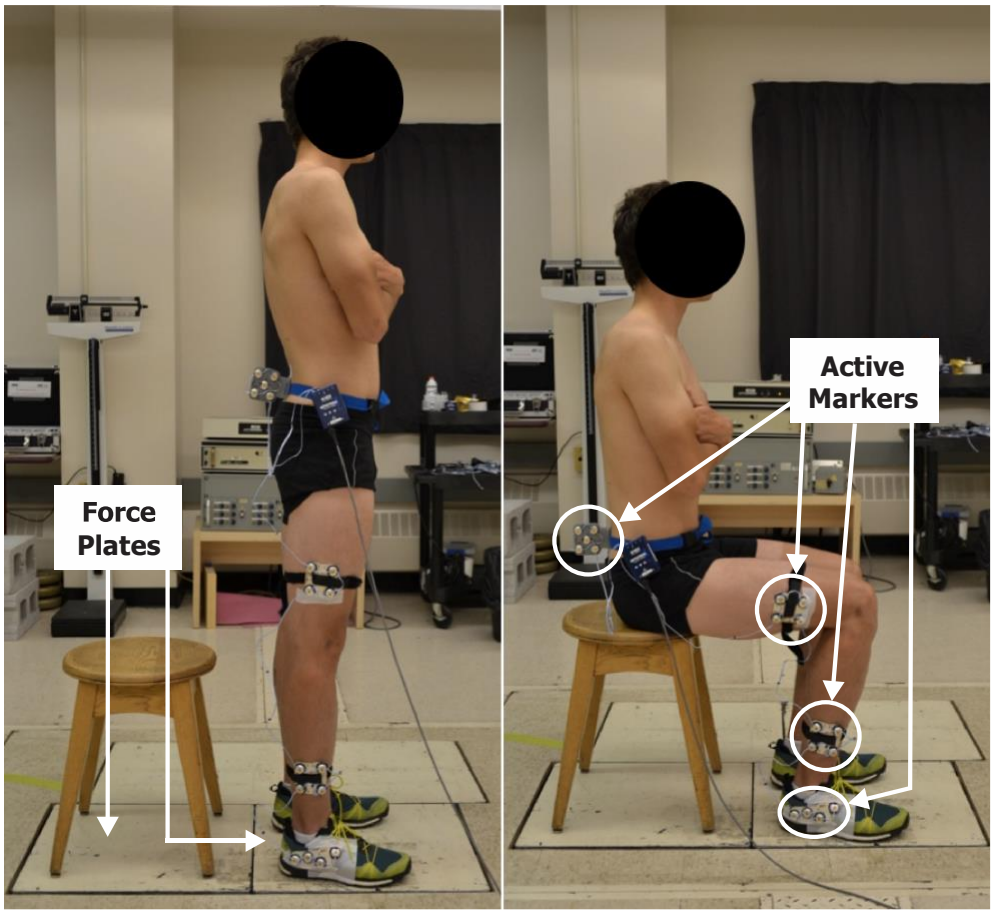

Figure 3. Photograph of the experimental measurements of human sitting and standing movement biomechanics with optical motion capture and synchronized force plates.

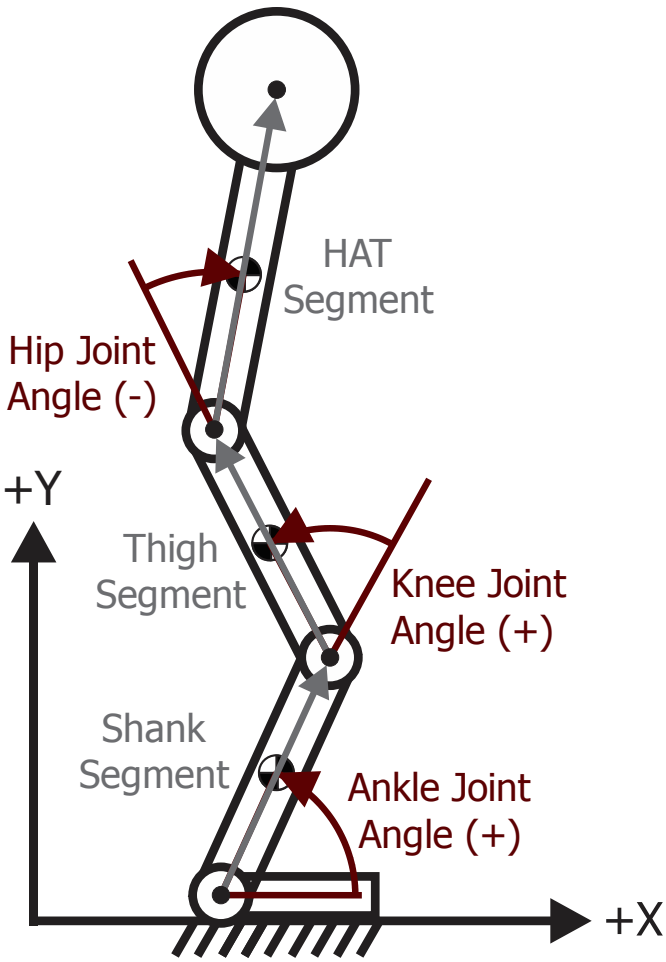

Figure 4. Schematic of the 2D human biomechanical model including hip, knee, and ankle joints and HAT, thigh, and shank body segments. The foot segment was fixed to the inertial ground frame.

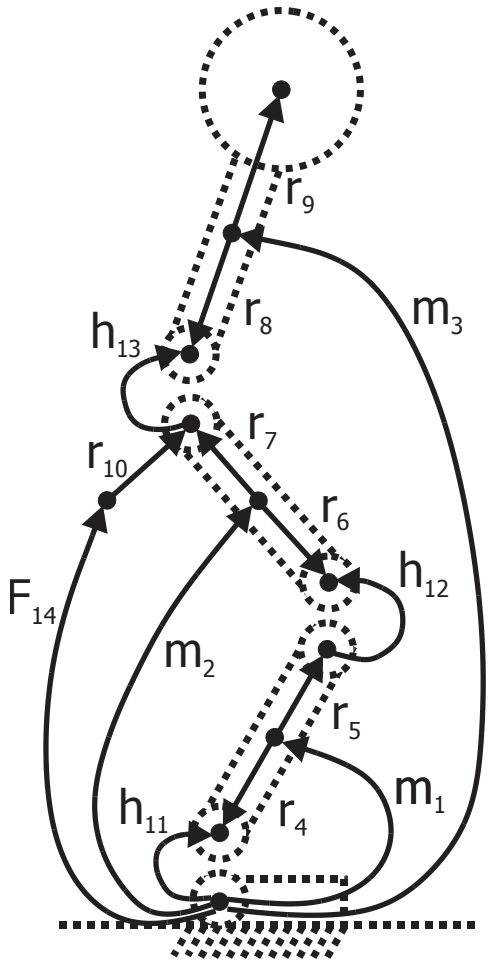

Figure 5. Linear graph representation of the human biomechanical model. Edges $m_{1\text{-}3}$ represent rigid body inertias. Elements $r_{4\text{-}9}$ are constant body-fixed position vectors. Edge r_{10} denotes the "seatoffset" position vector fixed to the thigh segment, $h_{11\text{-}13}$ are revolute joints, and F_{14} represents the external seat force. Bodyweight was lumped into edges $m_{1\text{-}3}$.

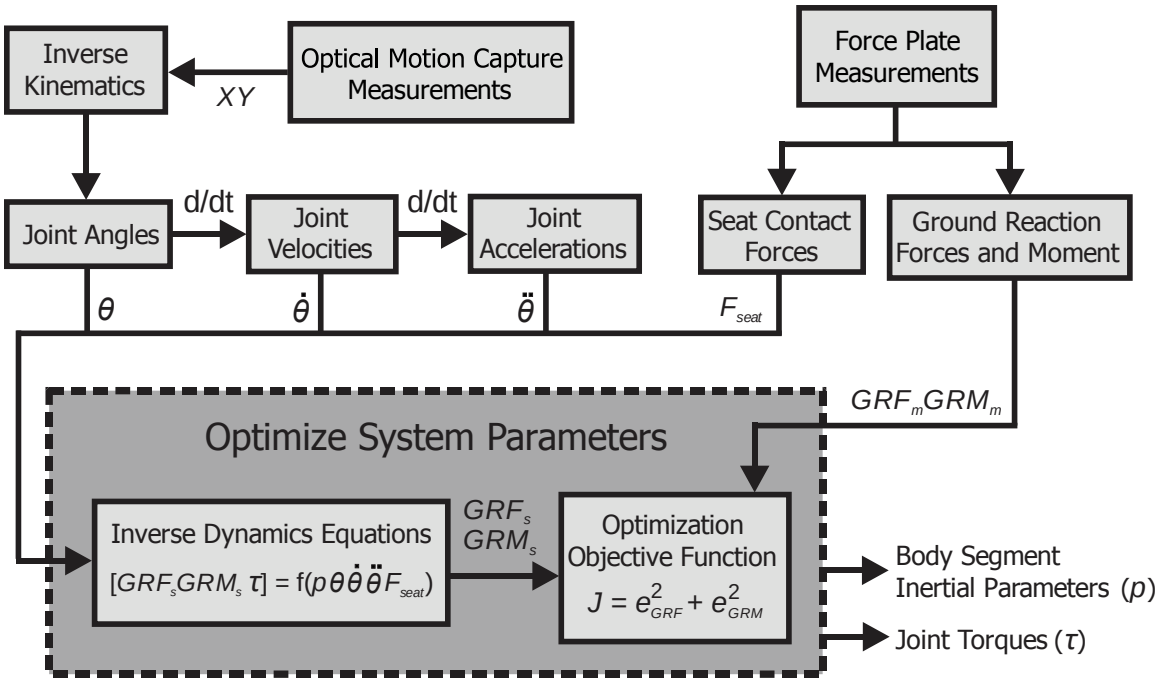

Figure 6. Flow diagram of the experimental and computational methods, including motion capture measurements, inverse kinematics and dynamics analyses, and subject-specific dynamic parameter identification.

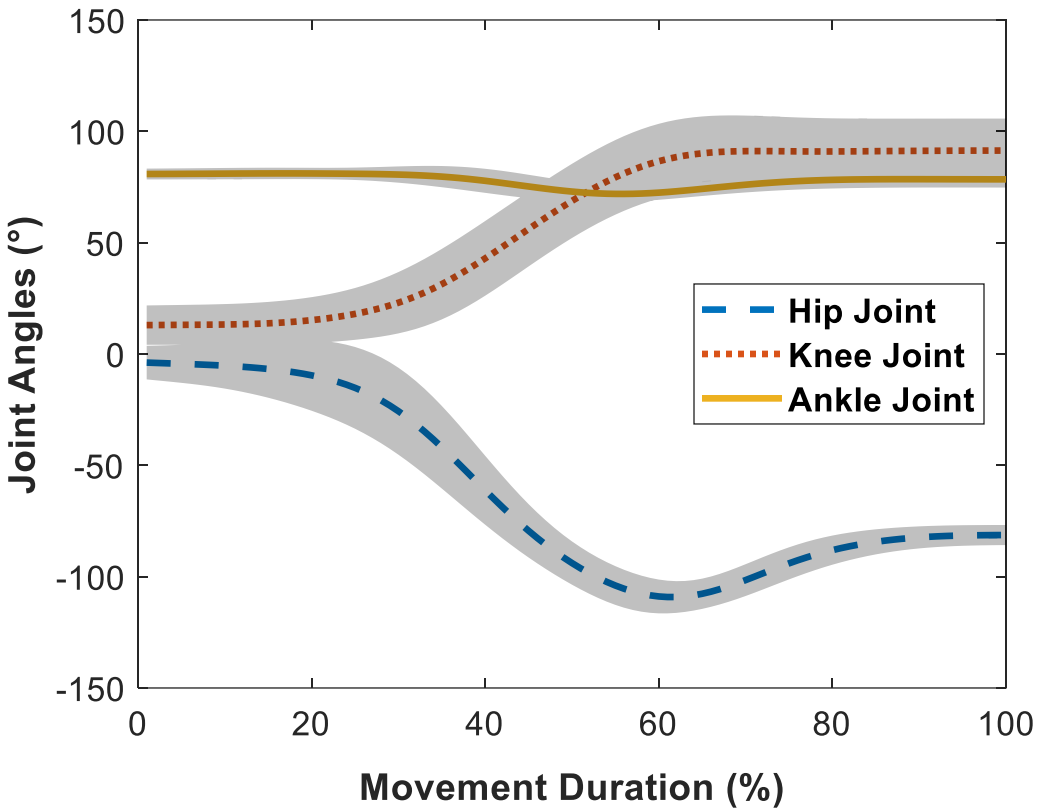

Figure 7. Calculated hip, knee, and ankle joint angles during stand-to-sit movements from inverse kinematics. The uncertainties represent ± one standard deviation across all participants (n=9) and trials (20 trials/participant).

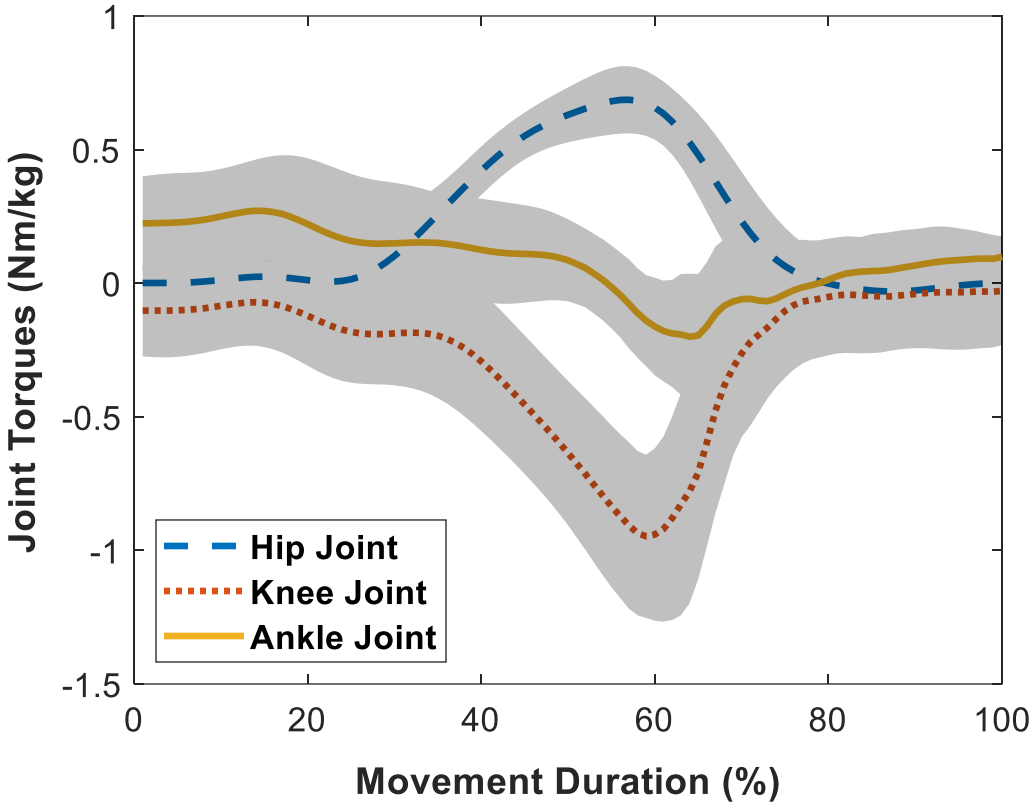

Figure 8. Calculated hip, knee, and ankle joint torques during stand-to-sit movements from inverse dynamic simulations, normalized to participant bodyweight. The uncertainties represent ± one standard deviation across all participants (n=9) and trials (20 trials/participant).

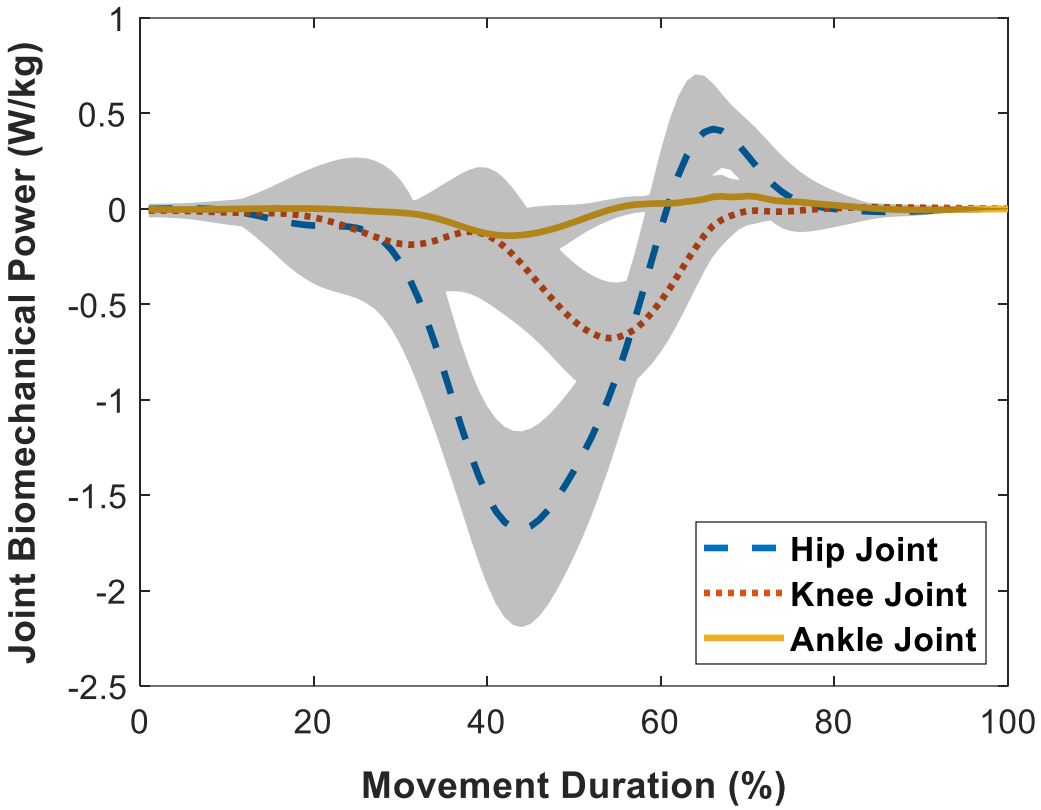

Figure 9. Estimated hip, knee, and ankle joint biomechanical powers during stand-to-sit movements, normalized to participant bodyweight. The uncertainties represent ± one standard deviation across all participants (n=9) and trials (20 trials/participant).

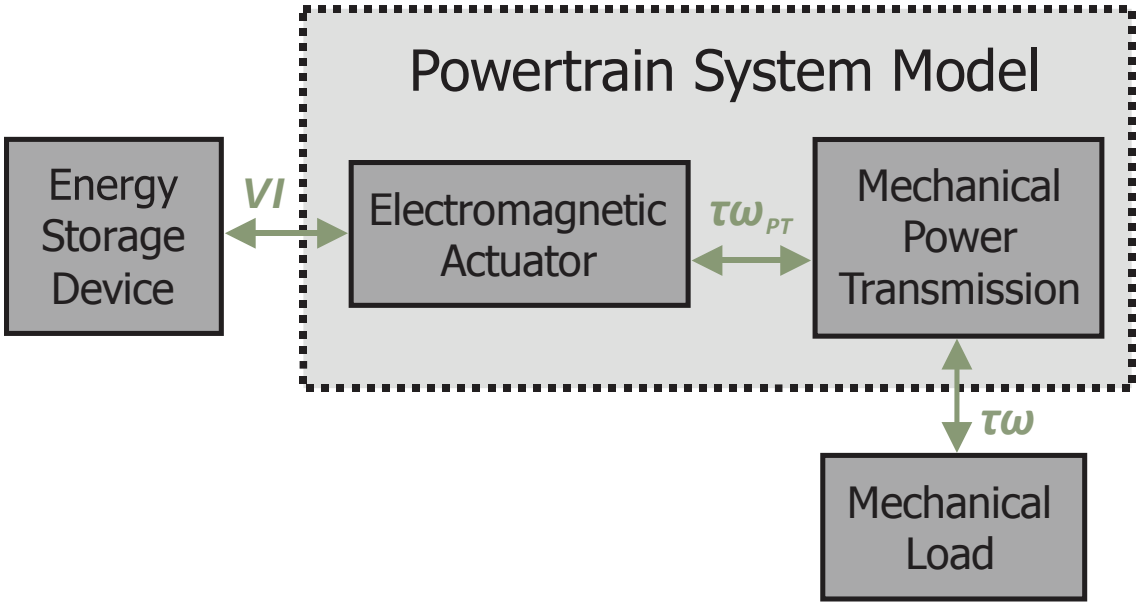

Figure 10. Example powertrain system model including an energy storage device, electromagnetic actuator, mechanical power transmission, and applied mechanical load (e.g., the modelled human knee joint biomechanics from the current research). Arrows represent the bidirectional flow of electrical (VI) and mechanical (τω) power during motoring and generating operations.

Table 1. Maximum and minimum hip, knee, and ankle joint angles, torques, and biomechanical powers during stand-to-sit movements. The uncertainties represent ± one standard deviation across all participants (n=9) and trials (20 trials/participant). Dynamic variables (i.e., net joint torques and biomechanical powers) were normalized to participant bodyweight.

	Joint Angle (°)	Joint Torque (Nm/kg)	Joint Power (W/kg)
Hip Maximum	-4.1 ± 7.2	0.7 ± 0.1	0.6 ± 0.2
Hip Minimum	-110.5 ± 7.1	-0.1 ± 0.1	-1.8 ± 0.5
Knee Maximum	92.4 ± 8.2	0.1 ± 0.2	0.1 ± 0.1
Knee Minimum	12.8 ± 12.2	-1.1 ± 0.3	-0.8 ± 0.3
Ankle Maximum	83.2 ± 2.8	0.4 ± 0.1	0.2 ± 0.1
Ankle Minimum	71.3 ± 3.5	-0.4 ± 0.2	-0.2 ± 0.1